applied sciences

MDPI

Article

Kinematic Calibration Method for Six-Hardpoint Positioning Mechanisms Using Optimal Measurement Pose

Zhiyuan Yu [1,2,*], Xiaoxia Wu [1] and Fuguo Wang [1]

[1] Changchun Institute of Optics, Fine Mechanics and Physics, Chinese Academy of Sciences, Changchun 130033, China; wuxiaoxia@ciomp.ac.cn (X.W.); wangfuguo@ciomp.ac.cn (F.W.)
[2] University of Chinese Academy of Sciences, Beijing 100049, China
* Correspondence: yuzhiyuan18@mails.ucas.edu.cn

Abstract: In this study, a kinematic calibration method is proposed. The method selects the optimal measurement poses based on the observability index O_1, and is used for six-hardpoint positioning mechanisms, which can identify and compensate for kinematic parameter errors of the mechanism. The calibration method is based on the derived error model. In order to improve the problem that measurement noise affects calibration accuracy, the proposed calibration method selects specific poses for calibration based on the observability index O_1, effectively improving the calibration accuracy. The reason for using O_1 is that we compared the performance of the five observability indices through simulation, and the results show that the calibration based on O_1 has the highest accuracy. In order to achieve pose selection based on observability indices, the DETMAX algorithm has been improved to achieve better performance of selection. Finally, an overall evaluation of the proposed calibration method is conducted, and the results show that the method can accurately identify kinematic parameter errors, with a fast error convergence speed. Compared with the traditional method, the proposed method has higher accuracy, reducing the mean position error by 78.4% and the mean attitude error by 70.6%. The proposed method is instrumental in the accurate kinematic calibration of six-hardpoint positioning mechanisms, and can effectively improve the accuracy of the mechanism, thus improving the pose accuracy of the primary mirror of the ground-based large aperture telescope.

Keywords: six-hardpoint positioning mechanism; parallel mechanism; kinematic calibration; observability index; optimal measurement pose

Citation: Yu, Z.; Wu, X.; Wang, F. Kinematic Calibration Method for Six-Hardpoint Positioning Mechanisms Using Optimal Measurement Pose. *Appl. Sci.* **2023**, *13*, 4824. https://doi.org/10.3390/app13084824

Academic Editor: Marco Troncossi

Received: 29 March 2023
Revised: 8 April 2023
Accepted: 10 April 2023
Published: 12 April 2023

1. Introduction

The six-hardpoint positioning mechanism is applied to the active support system of ground-based large aperture telescopes, which is used for primary mirror positioning and pose adjustment. It has been applied to some large aperture telescopes, such as the Large Binocular Telescope [1,2], Vera C. Rubin Observatory (formerly known as the Large Synoptic Survey Telescope) [3,4], and the Giant Magellan Telescope [5,6]. Ensuring the accuracy of the pose of the primary mirror is very important for telescopes, which directly affects the imaging quality of telescopes. Once the pose error of the primary mirror exceeds the error range, it will not only lead to various aberrations, but also cause misalignment of the optical and mechanical axes, leading to the instability of the imaging position, which has a disastrous impact on the performance of the telescope [7,8]. Therefore, the six-hardpoint positioning mechanism must have very high kinematic accuracy, so as to ensure that the primary mirror can be accurately positioned in a predetermined pose during telescope observation.

However, in practice, the accuracy of six-hardpoint positioning mechanisms can significantly deteriorate due to the existence of kinematic parameter errors. Due to the complex structure of the six-hardpoint positioning mechanism, it is inevitable to introduce

kinematic parameter errors during the manufacturing and assembly process. Kinematic parameter errors lead to deviations between the actual and theoretical kinematic models of the mechanism, which then leads to the pose error of the primary mirror, and reduces the imaging quality of the telescope. Therefore, measures must be taken to correct the kinematic parameter errors or compensate the kinematic parameter errors in the kinematic model. There are up to 42 kinematic parameter errors in the six-hardpoint positioning mechanism, which are difficult to measure directly, and therefore difficult to achieve direct correction.

This paper attempts to solve this problem via the proposed calibration method for the six-hardpoint positioning mechanism. Generally, kinematic calibration includes four steps: (i) error modeling, (ii) pose measurement, (iii) error identification, and (iv) error compensation [9,10]. Kinematic calibration is widely used for various robots, which can effectively and economically improve the kinematic accuracy of robots without changing hardware. Firstly, the relationship between the kinematic parameter errors of the robot and the pose errors of the robot end effector is established through an error model, so the kinematic parameter errors can be solved and identified by measuring the actual poses of the end effector. Then, the theoretical kinematic parameters are corrected using kinematic parameter errors. Finally, a new kinematic model is established based on the corrected kinematic parameters. The new kinematic model is closer to the actual kinematic model and achieves error compensation. Kinematic calibration solves the problem of kinematic parameter errors and improves the accuracy of the robot. Calibration is applied to various robots, including tri-pyramid parallel robot [11], industrial robot [12], airborne heavy-duty mechanical arm [13], Stewart platform [14,15], hybrid manipulators [16], 7-DoF hybrid robots, etc. [17].

To perform kinematic calibration of six-hardpoint positioning mechanisms, the measurement of the poses of the primary mirror is an important step. The accuracy of calibration can only be guaranteed by obtaining accurate poses of the primary mirror. However, the measurement values of the pose always contain some measurement noise. The causes of the noise include not only errors in the measurement equipment, but also errors in the process of pose resolving. The inevitable measurement noise will reduce the accuracy of calibration. In response to the problem of measurement noise, five observability indices have been proposed in succession, namely O_1, O_2, O_3, O_4, and O_5 [18–23]. Research has shown that if the measurement poses for kinematic calibration are selected based on the criteria for maximizing the observability index, the impact of measurement noise can be reduced and the accuracy of calibration can be improved [24].

However, there are as many as five commonly used observability indices, so which one to choose for calibration of six-hardpoint positioning mechanisms has become another issue that needs to be addressed. Saputra et al. [25] proposed a method to calibrate a parallel robot by using a measurement system specially installed on the external fixed frame, and then compared the performance of the first four observability indices. The results show that O_4 has relatively good performance. Sun et al. [23] studied the physical meaning and properties of observability indices and carried out mathematical analysis. O_1 and O_3 were described as relatively good choices. Horne and Notash [26] investigated the performances of the observability indices through the simulation of a 2-DOF planar manipulator. The simulation results revealed that O_5 and O_3 had good and bad performances, respectively. Zhou et al. [27] studied the performances of the observability indices through the calibration of a 2-link planar robot, and O_4 is the best observability index. To sum up, there are different viewpoints on the performance of the observability indices at present, and further research is needed.

In order to improve the accuracy of the proposed calibration method for six-hardpoint positioning mechanisms, this paper attempts to find the most suitable observability index for this mechanism. Therefore, many simulations of calibration have been conducted for this mechanism, and the performance of the five observability indices have been compared. Finally, the best performance observability index O_1 has been obtained. Specific algorithms are required for measurement pose selection based on O_1, such as genetic algorithms

and DETMAX. This paper improves the DETMAX algorithm by setting a tabu list in the algorithm, which improves the problem that DETMAX is greatly affected by initial values, and the problem that DETMAX easily converges to the local maximum value.

Finally, in order to validate the proposed kinematic calibration method for six-hardpoint positioning mechanisms, an overall evaluation of the method was conducted. Comparing the effectiveness and accuracy of traditional calibration method and the proposed calibration methods, the results show that the proposed method has higher effectiveness and accuracy compared to traditional methods.

The main contributions of this paper are as follows: (1) A kinematic calibration method is proposed which selects the optimal measurement poses based on the observability index O_1. The method can not only identify and compensate for the kinematic errors of the six-hardpoint positioning mechanism, but can also have higher calibration accuracy than traditional methods. (2) This paper improves the DETMAX algorithm for selecting the optimal measurement pose. Based on the DETMAX algorithm, a tabu list is added, effectively improving its problems of easy convergence to a local optimal solution and being greatly affected by initial values. (3) Through many simulations of calibration, this paper compares the performance of observability indices in the calibration of six-hardpoint positioning mechanisms, and ultimately obtains the best performance indicator. The proposed calibration method is based on this index. The simulation is equivalent to 2000 calibrations, so the conclusions are universal and statistically significant.

The content of the rest of this article is arranged as follows: Section 2 introduces the mathematical model and derivation process of the six-hardpoint positioning mechanism. Section 3 introduces observability indices and the algorithm used to select optimal measurement poses. Section 4 compares the performance of the observability indices, including the method of numerical simulation of calibration and calibration accuracy evaluation methods. Section 5 evaluates the proposed calibration method. Finally, the study is concluded in Section 6.

2. Six-Hardpoint Positioning Mechanism and Its Mathematical Model

The six-hardpoint positioning mechanism is used to adjust and maintain the pose of the large aperture primary mirror. It forms a primary mirror positioning system with the primary mirror and mirror cell, and is a subsystem of the pneumatic active support system for the primary mirror of the large aperture ground-based telescope. As shown in Figure 1, the six-hardpoint positioning mechanism consists of six identical hardpoints, one end of the hardpoint is connected to the primary mirror back plate at A_1 to A_6 through a flexible hinge, and the other end is connected to the mirror cell at B_1 to B_6 through a flexible hinge. The hardpoint can be considered as a displacement actuator with high axial stiffness, so the kinematic principle of the mechanism is similar to that of a Stewart platform. Adjusting the lengths of the hardpoints can realize the adjustment of the pose of the primary mirror relative to the mirror cell. When the lengths of all hardpoints are maintained, the six-hardpoint positioning mechanism completely limits the degrees of freedom of the primary mirror to maintain the pose of the primary mirror.

The mathematical model includes kinematic models and an error model. Kinematic models include forward and inverse kinematic models. The forward kinematic model refers to obtaining the pose of the primary mirror through the length of the hardpoint, and the inverse model refers to obtaining the lengths through the pose. Both the forward and inverse model need to be used in calibration. The error model provides the relationship between kinematic parameter errors of the mechanism and pose errors of the primary mirror, which is one of the contents of kinematic calibration.

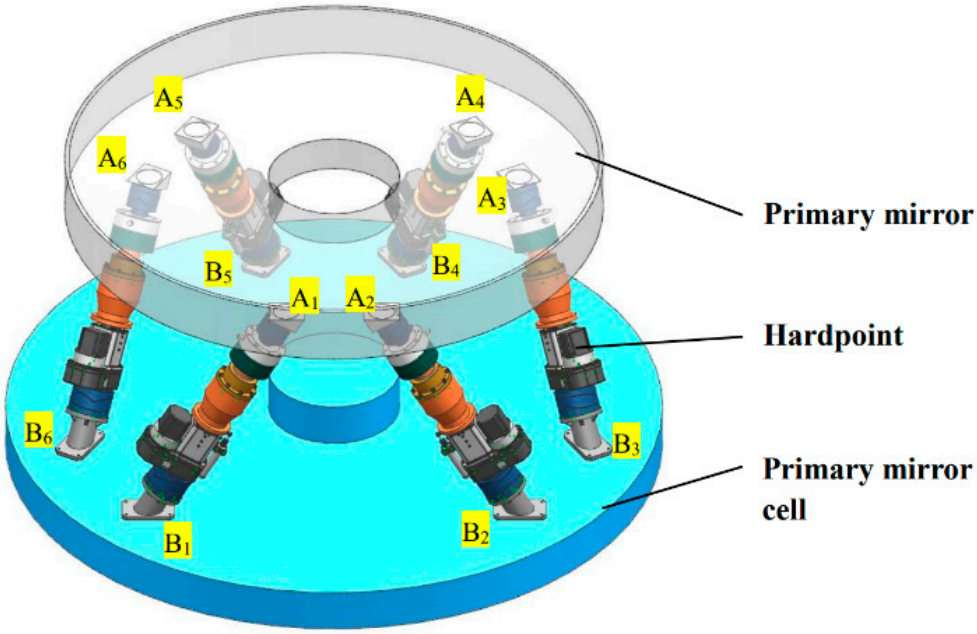

Figure 1. Three-dimensional model of the six-hardpoint positioning mechanism and the primary mirror positioning system. For clarity of expression, the primary mirror has been changed to translucent, and the structure of the mirror cell has been simplified.

2.1. Kinematic Model of Six-Hardpoint Positioning Mechanisms

2.1.1. Inverse Kinematic Model

The structural diagram of the six-hardpoint positioning mechanism is shown in Figure 2, which is a simplified version of Figure 1. Figure 2a shows the initial pose state of the mechanism, and Figure 2b shows the mechanism in the state after a pose adjustment. When considering the primary mirror as a rigid body, it has 6 degrees of freedom, so the pose of the primary mirror can be determined through 6 coordinate parameters, using $\boldsymbol{q} = [x\ y\ z\ \alpha\ \beta\ \gamma]^{\mathrm{T}}$ which represents the pose of the primary mirror. $\boldsymbol{q}$ can be decomposed into a position vector $\boldsymbol{t} = [x\ y\ z]^{\mathrm{T}}$ and an attitude vector $\boldsymbol{s} = [\alpha\ \beta\ \gamma]^{\mathrm{T}}$. According to the geometric relationship in Figure 2, the inverse kinematic model of the six-hardpoint positioning mechanism can be directly obtained:

$$\boldsymbol{l}_i = \boldsymbol{t} + \boldsymbol{R}\boldsymbol{a}_i - \boldsymbol{b}_i \tag{1}$$

where i = 1, 2,..., 6, corresponding to the six hardpoints. $\boldsymbol{l}_i$ is the vector in the direction of the hardpoint, and the norm of the vector is the length of the hardpoint. $\boldsymbol{t}$ is the position vector of the primary mirror and the coordinate of the coordinate origin O_1 in the O-xyz. $\boldsymbol{a}_\mathrm{i}$ is the coordinate of the upper support point $\mathrm{A_i}$ in the coordinate system O_1-$\mathrm{x_1y_1z_1}$, and $\boldsymbol{b}_\mathrm{i}$ is the coordinate of the lower support point $\mathrm{B_i}$ in the coordinate system O-xyz (O_1 and O_2 here refer to the coordinate origins, which are independent of the observability indices O_1 and O_2). $\boldsymbol{R}$ is the rotation matrix and is represented as follows:

$$\boldsymbol{R} = \begin{bmatrix} \cos\gamma\cos\beta & \cos\gamma\sin\beta\sin\alpha - \sin\gamma\cos\alpha & \cos\gamma\sin\beta\cos\alpha + \sin\gamma\sin\alpha \\ \sin\gamma\cos\beta & \sin\gamma\sin\beta\sin\alpha + \cos\gamma\cos\alpha & \sin\gamma\sin\beta\cos\alpha - \cos\gamma\sin\alpha \\ -\sin\beta & \cos\beta\sin\alpha & \cos\beta\cos\alpha \end{bmatrix} \tag{2}$$

where α, β, and γ are the rotation angles of the primary mirror around the coordinate axes $\mathrm{x_2}$, $\mathrm{y_2}$, $\mathrm{z_2}$, which are elements in the attitude vector $\boldsymbol{s} = [\alpha\ \beta\ \gamma]^{\mathrm{T}}$. The inverse kinematics model can calculate the length and direction of each hardpoint through the primary mirror pose.

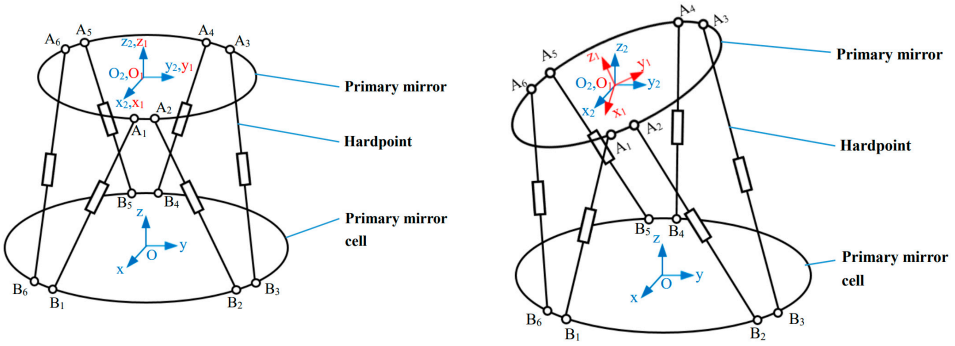

(**a**) (**b**)

Figure 2. Structural diagram of the six-hardpoint positioning mechanism. (**a**) The mechanism in the initial pose; (**b**) The mechanism in the state after a pose adjustment.

2.1.2. Forward Kinematic Model

The forward kinematic model is used to solve the pose of the primary mirror through the given lengths of the six hardpoints, based on the Gauss–Newton iteration method. According to the inverse kinematic Equation (1), the length h_i of the hardpoint is:

$$\begin{aligned} h_i &= |\boldsymbol{l}_i| \\ &= \sqrt{\boldsymbol{l}_i^T \boldsymbol{l}_i} \\ &= \sqrt{(\boldsymbol{t} + \boldsymbol{R}\boldsymbol{a}_i - \boldsymbol{b}_i)^T (\boldsymbol{t} + \boldsymbol{R}\boldsymbol{a}_i - \boldsymbol{b}_i)} \end{aligned} \tag{3}$$

where i = 1, 2,..., 6. Equation (3) is the forward kinematic equation, which is classified as a nonlinear equation and is difficult to solve directly. Therefore, according to the Gauss–Newton iteration method, the following function $F(\boldsymbol{q})$ is constructed:

$$F(\boldsymbol{q}) = \sum_{i=1}^{6} \left[h_i - \sqrt{(\boldsymbol{t} + \boldsymbol{R}\boldsymbol{a}_i - \boldsymbol{b}_i)^T (\boldsymbol{t} + \boldsymbol{R}\boldsymbol{a}_i - \boldsymbol{b}_i)} \right]^2 \tag{4}$$

In this way, the problem of solving the nonlinear equation is transformed into the problem of finding the pose $\boldsymbol{q}$ of the primary mirror that minimizes $F(\boldsymbol{q})$. It can be solved by the least squares method. For the convenience of calculation, make:

$$f_i(\boldsymbol{q}) = h_i - \sqrt{(\boldsymbol{t} + \boldsymbol{R}\boldsymbol{a}_i - \boldsymbol{b}_i)^T (\boldsymbol{t} + \boldsymbol{R}\boldsymbol{a}_i - \boldsymbol{b}_i)} \tag{5}$$

$$\boldsymbol{f}(\boldsymbol{q}) = [f_1(\boldsymbol{q}), f_2(\boldsymbol{q}), f_3(\boldsymbol{q}), f_4(\boldsymbol{q}), f_5(\boldsymbol{q}), f_6(\boldsymbol{q})]^T \tag{6}$$

Then, substituting Equation (6) into Equation (4) yields:

$$F(\boldsymbol{q}) = \boldsymbol{f}(\boldsymbol{q})^T \boldsymbol{f}(\boldsymbol{q}) \tag{7}$$

The iteration formula according to the Gauss–Newton iteration method is:

$$\boldsymbol{q}_{k+1} = \boldsymbol{q}_k - \left[(\boldsymbol{J}_k)^T \boldsymbol{J}_k \right]^{-1} (\boldsymbol{J}_k)^T \boldsymbol{r}_k \tag{8}$$

where:

$$\boldsymbol{J}_k = \begin{bmatrix} \frac{\partial f_1(\boldsymbol{q})}{\partial x} & \frac{\partial f_1(\boldsymbol{q})}{\partial y} & \frac{\partial f_1(\boldsymbol{q})}{\partial z} & \frac{\partial f_1(\boldsymbol{q})}{\partial \alpha} & \frac{\partial f_1(\boldsymbol{q})}{\partial \beta} & \frac{\partial f_1(\boldsymbol{q})}{\partial \gamma} \\ \frac{\partial f_2(\boldsymbol{q})}{\partial x} & \frac{\partial f_2(\boldsymbol{q})}{\partial y} & \frac{\partial f_2(\boldsymbol{q})}{\partial z} & \frac{\partial f_2(\boldsymbol{q})}{\partial \alpha} & \frac{\partial f_2(\boldsymbol{q})}{\partial \beta} & \frac{\partial f_2(\boldsymbol{q})}{\partial \gamma} \\ \frac{\partial f_3(\boldsymbol{q})}{\partial x} & \frac{\partial f_3(\boldsymbol{q})}{\partial y} & \frac{\partial f_3(\boldsymbol{q})}{\partial z} & \frac{\partial f_3(\boldsymbol{q})}{\partial \alpha} & \frac{\partial f_3(\boldsymbol{q})}{\partial \beta} & \frac{\partial f_3(\boldsymbol{q})}{\partial \gamma} \\ \frac{\partial f_4(\boldsymbol{q})}{\partial x} & \frac{\partial f_4(\boldsymbol{q})}{\partial y} & \frac{\partial f_4(\boldsymbol{q})}{\partial z} & \frac{\partial f_4(\boldsymbol{q})}{\partial \alpha} & \frac{\partial f_4(\boldsymbol{q})}{\partial \beta} & \frac{\partial f_4(\boldsymbol{q})}{\partial \gamma} \\ \frac{\partial f_5(\boldsymbol{q})}{\partial x} & \frac{\partial f_5(\boldsymbol{q})}{\partial y} & \frac{\partial f_5(\boldsymbol{q})}{\partial z} & \frac{\partial f_5(\boldsymbol{q})}{\partial \alpha} & \frac{\partial f_5(\boldsymbol{q})}{\partial \beta} & \frac{\partial f_5(\boldsymbol{q})}{\partial \gamma} \\ \frac{\partial f_6(\boldsymbol{q})}{\partial x} & \frac{\partial f_6(\boldsymbol{q})}{\partial y} & \frac{\partial f_6(\boldsymbol{q})}{\partial z} & \frac{\partial f_6(\boldsymbol{q})}{\partial \alpha} & \frac{\partial f_6(\boldsymbol{q})}{\partial \beta} & \frac{\partial f_6(\boldsymbol{q})}{\partial \gamma} \end{bmatrix} \tag{9}$$

$$\boldsymbol{r}_k = \boldsymbol{f}(\boldsymbol{q}) = [f_1(\boldsymbol{q}), f_2(\boldsymbol{q}), f_3(\boldsymbol{q}), f_4(\boldsymbol{q}), f_5(\boldsymbol{q}), f_6(\boldsymbol{q})]^T \tag{10}$$

Since the Jacobian matrix $\boldsymbol{J}_\mathrm{k}$ is a reversible matrix, Equation (8) can be simplified to:

$$\boldsymbol{q}_{k+1} = \boldsymbol{q}_k - \boldsymbol{J}_k{}^{-1}\boldsymbol{r}_k \tag{11}$$

The steps of the iterative method of the forward kinematic model are as follows:

① Given an initial value $\boldsymbol{q}_1$, and iteration accuracy $\varepsilon > 0$, let k = 1.

② Substitute $\boldsymbol{q}_\mathrm{k}$ and the lengths h_i of hardpoints into $\boldsymbol{J}_\mathrm{k}$, $\boldsymbol{J}_\mathrm{k}{}^{-1}$, and $\boldsymbol{r}_\mathrm{k}$, and then calculate $\boldsymbol{q}_{\mathrm{k+1}}$.

③ If $|\boldsymbol{q}_{\mathrm{k+1}} - \boldsymbol{q}_\mathrm{k}| < \varepsilon$ is satisfied, then terminate the iterations. Otherwise set k = k + 1, and repeat step ②.

④ When the iterations are terminated, $\boldsymbol{q}_{\mathrm{k+1}}$ represents the pose of the primary mirror obtained from the forward kinematic model.

2.2. Error Model of Six-Hardpoint Positioning Mechanism

For any robot, error modeling is an important part of kinematic calibration, which requires solving the problems of which errors should be modeled and how to model them. For the six-hardpoint positioning mechanism, factors that affect the pose accuracy of the primary mirror include both geometric errors (such as kinematic parameter errors) and non-geometric errors (such as gravitational deformation and thermal expansion of materials). The kinematic calibration in this study specifically investigates the kinematic parameter errors. The error model is established based on the inverse kinematic Equation (1), which can be rewritten as:

$$|\boldsymbol{t} + \boldsymbol{R}\boldsymbol{a}_i - \boldsymbol{b}_i|^2 - {h_i}^2 = 0 \tag{12}$$

where $\boldsymbol{a}_\mathrm{i}$, $\boldsymbol{b}_\mathrm{i}$, and h_i are collectively referred to as kinematic parameters. $\boldsymbol{a}_\mathrm{i}$ and $\boldsymbol{b}_\mathrm{i}$ can be defined as follows:

$$\boldsymbol{a}_i = \begin{bmatrix} x_{Ai} & y_{Ai} & z_{Ai} \end{bmatrix}^T \tag{13}$$

$$\boldsymbol{b}_i = \begin{bmatrix} x_{Bi} & y_{Bi} & z_{Bi} \end{bmatrix}^T \tag{14}$$

where i = 1, 2,..., 6, with each i corresponding to a hardpoint. Additionally, there are 7 kinematic parameters related to each hardpoint, of which 3 represent the position of the upper support point, 3 represent the position of the lower support point, and 1 represents the length of the hardpoint. Therefore, the total number of kinematic parameters is 42, and $\boldsymbol{C}$ represents the vector composed of all kinematic parameters:

$$\boldsymbol{C} = [\mathrm{x}_{A1} \quad y_{A1} \quad z_{A1} \quad h_1 \quad x_{B1} \quad y_{B1} \quad z_{B1} \quad \cdots \quad x_{A6} \quad y_{A6} \quad z_{A6} \quad h_6 \quad x_{B6} \quad y_{B6} \quad z_{B6} \ ]^T \tag{15}$$

In addition to the above kinematic parameters, Equation (12) also includes the relevant parameter $\boldsymbol{q}$, that is the pose of the primary mirror. Therefore, Equation (12) can be rewritten in the following form:

$$f_i(x, y, z, \alpha, \beta, \gamma, x_{Ai}, y_{Ai}, z_{Ai}, h_i, x_{Bi}, y_{Bi}, z_{Bi}) = 0 \tag{16}$$

Through complete differentiation, Equation (16) can be transformed into:

$$\begin{aligned}&\frac{\partial f_i}{\partial x}dx+\frac{\partial f_i}{\partial y}dy+\frac{\partial f_i}{\partial z}dz+\frac{\partial f_i}{\partial \alpha}d\alpha+\frac{\partial f_i}{\partial \beta}d\beta+\frac{\partial f_i}{\partial \gamma}d\gamma+\frac{\partial f_i}{\partial x_{Ai}}dx_{Ai}+\frac{\partial f_i}{\partial y_{Ai}}dy_{Ai}\\&+\frac{\partial f_i}{\partial z_{Ai}}dz_{Ai}+\frac{\partial f_i}{\partial d_i}dh_i+\frac{\partial f_i}{\partial x_{Bi}}dx_{Bi}+\frac{\partial f_i}{\partial y_{Bi}}dy_{Bi}+\frac{\partial f_i}{\partial z_{Bi}}dz_{Bi}=0\end{aligned} \tag{17}$$

which can be expressed in matrix form as follows:

$$\boldsymbol{J}_1 d\boldsymbol{q}=\boldsymbol{J}_2 d\boldsymbol{C} \tag{18}$$

where:

$$\boldsymbol{J}_1=\begin{bmatrix}\frac{\partial f_1}{\partial x}&\frac{\partial f_1}{\partial y}&\frac{\partial f_1}{\partial z}&\frac{\partial f_1}{\partial \alpha}&\frac{\partial f_1}{\partial \beta}&\frac{\partial f_1}{\partial \gamma}\\ \frac{\partial f_2}{\partial x}&\frac{\partial f_2}{\partial y}&\frac{\partial f_2}{\partial z}&\frac{\partial f_2}{\partial \alpha}&\frac{\partial f_2}{\partial \beta}&\frac{\partial f_2}{\partial \gamma}\\ \frac{\partial f_3}{\partial x}&\frac{\partial f_3}{\partial y}&\frac{\partial f_3}{\partial z}&\frac{\partial f_3}{\partial \alpha}&\frac{\partial f_3}{\partial \beta}&\frac{\partial f_3}{\partial \gamma}\\ \frac{\partial f_4}{\partial x}&\frac{\partial f_4}{\partial y}&\frac{\partial f_4}{\partial z}&\frac{\partial f_4}{\partial \alpha}&\frac{\partial f_4}{\partial \beta}&\frac{\partial f_4}{\partial \gamma}\\ \frac{\partial f_5}{\partial x}&\frac{\partial f_5}{\partial y}&\frac{\partial f_5}{\partial z}&\frac{\partial f_5}{\partial \alpha}&\frac{\partial f_5}{\partial \beta}&\frac{\partial f_5}{\partial \gamma}\\ \frac{\partial f_6}{\partial x}&\frac{\partial f_6}{\partial y}&\frac{\partial f_6}{\partial z}&\frac{\partial f_6}{\partial \alpha}&\frac{\partial f_6}{\partial \beta}&\frac{\partial f_6}{\partial \gamma}\end{bmatrix} \tag{19}$$

$$d\boldsymbol{q}=\begin{bmatrix}dx&dy&dz&d\alpha&d\beta&d\gamma\end{bmatrix}^T \tag{20}$$

$$\boldsymbol{J}_2=\begin{bmatrix}\frac{\partial f_1}{\partial x_{A1}}&\frac{\partial f_1}{\partial y_{A1}}&\frac{\partial f_1}{\partial z_{A1}}&\frac{\partial f_1}{\partial h_1}&\frac{\partial f_1}{\partial x_{B1}}&\frac{\partial f_1}{\partial y_{B1}}&\frac{\partial f_1}{\partial z_{B1}}&\cdots&&&0&&&\\ &&&\vdots&&&&\ddots&&&\vdots&&&\\ &&&0&&&&\cdots&\frac{\partial f_6}{\partial x_{A6}}&\frac{\partial f_6}{\partial y_{A6}}&\frac{\partial f_6}{\partial z_{A6}}&\frac{\partial f_6}{\partial h_6}&\frac{\partial f_6}{\partial x_{B6}}&\frac{\partial f_6}{\partial y_{B6}}&\frac{\partial f_6}{\partial z_{B6}}\end{bmatrix} \tag{21}$$

$$d\boldsymbol{C}=\begin{bmatrix}dx_{A1}&dy_{A1}&dz_{A1}&dh_1&dx_{B1}&dy_{B1}&dz_{B1}&\cdots&dx_{A6}&dy_{A6}&dz_{A6}&dh_6&dx_{B6}&dy_{B6}&dz_{B6}\end{bmatrix}^T \tag{22}$$

where $\boldsymbol{J}_1$ is 6×6 matrix and $\boldsymbol{J}_2$ is 6×42 matrix. d$\boldsymbol{q}$ represents the pose errors of the primary mirror, which is a 6×1 vector, and d$\boldsymbol{C}$ represents the errors of kinematic parameters, which is a 42×1 vector. Since $\boldsymbol{J}_1$ is a reversible matrix, Equation (19) can be transformed as follows:

$$d\boldsymbol{q}={\boldsymbol{J}_1}^{-1}\boldsymbol{J}_2 d\boldsymbol{C}=\boldsymbol{J}_b d\boldsymbol{C} \tag{23}$$

where $\boldsymbol{J}_\mathrm{b}$ is a 6×42 matrix, and $\boldsymbol{J}_\mathrm{b}$ is a function of $\boldsymbol{q}$, $\boldsymbol{H}$, $\boldsymbol{A}$, $\boldsymbol{B}$, with $\boldsymbol{H}$, $\boldsymbol{A}$, $\boldsymbol{B}$ expressed as follows:

$$\boldsymbol{H}=\begin{bmatrix}h_1&h_2&h_3&h_4&h_5&h_6\end{bmatrix}^T \tag{24}$$

$$\boldsymbol{A}=\begin{bmatrix}\boldsymbol{a}_1&\boldsymbol{a}_2&\boldsymbol{a}_3&\boldsymbol{a}_4&\boldsymbol{a}_5&\boldsymbol{a}_6\end{bmatrix}^T \tag{25}$$

$$\boldsymbol{B}=\begin{bmatrix}\boldsymbol{b}_1&\boldsymbol{b}_2&\boldsymbol{b}_3&\boldsymbol{b}_4&\boldsymbol{b}_5&\boldsymbol{b}_6\end{bmatrix}^T \tag{26}$$

Equation (23) is the preliminary error model of the six-hardpoint positioning mechanism. The model provides the relationship between the pose error vector d$\boldsymbol{q}$ of the primary mirror and the kinematic parameter error vector d$\boldsymbol{C}$ of the six-hardpoint positioning mechanism. However, Equation (23) cannot be solved directly, because d$\boldsymbol{q}$ contains 6 parameters, whereas d$\boldsymbol{C}$ contains 42 parameters to be solved. Therefore, at least 7 error equations must be combined to achieve the solution, so at least 7 poses must be measured. The target pose of the primary mirror used in the calibration is called the measurement pose. Set the number of measurement poses as n (where $n\geq 7$), and combine n error equations to obtain:

$$d\boldsymbol{q}_B=\boldsymbol{J}_B d\boldsymbol{C} \tag{27}$$

where:

$$d\boldsymbol{q}_B = \begin{bmatrix} d\boldsymbol{q}_1 & d\boldsymbol{q}_2 & \cdots & d\boldsymbol{q}_n \end{bmatrix}^T \tag{28}$$

$$\boldsymbol{J}_B = \begin{bmatrix} \boldsymbol{J}_{b1} & \boldsymbol{J}_{b2} & \cdots & \boldsymbol{J}_{bn} \end{bmatrix}^T \tag{29}$$

where d$\boldsymbol{q}_\mathrm{B}$ is a $6n \times 1$ vector, and $\boldsymbol{J}_\mathrm{B}$ is a $6n \times 42$ matrix. $\boldsymbol{J}_\mathrm{B}$ is called identification Jacobian matrix. Equation (27) is the final error model of the six-hardpoint positioning mechanism. The kinematic calibration of a six-hardpoint positioning mechanism can be carried out based on the error model. The n ($n \geq 7$) poses of the primary mirror are measured and the positional errors are calculated, then the least square method is used to solve Equation (27) to obtain the kinematic parameter error d$\boldsymbol{C}$.

Although kinematic calibration can achieve the solution and compensation of kinematic parameter errors, the accuracy of calibration is affected by measurement noise. Equipment such as a length gauge, a laser tracker, an LVDT, and a measuring arm can be used to measure the pose of the primary mirror, all of which have certain errors. In addition, the process of pose resolving can also cause errors [28–31]. The above factors cause a certain amount of measurement noise in the pose error d$\boldsymbol{q}_\mathrm{B}$, which reduces the compensation accuracy of the kinematic parameter error d$\boldsymbol{C}$, and thus affects the accuracy of calibration.

3. Selecting Optimal Measurement Poses Based on Observability Index

3.1. Introduction to Observability Indices

Observability indices are used to select optimal measurement poses. Using these poses for calibration can improve the problem of measurement noise reducing calibration accuracy. When the measurement noise level is maintained, selecting different measurement poses for robot calibration will result in different calibration accuracies [22]. Theoretically, it is possible to use multiple sets of poses spread throughout the workspace of the robot for calibration, and then retain the set with the highest accuracy after calibration. However, in order to spread throughout the entire workspace, multiple sets of poses have to be selected, as well as perform many calibrations, which is time-consuming, labor-intensive, and generally difficult to operate in practice. Therefore, to efficiently select suitable measurement poses for kinematic calibration, five observability indices, O_1~O_5, have been proposed [18–23]. For several groups of measurement poses, the group with a larger observability index is more likely to achieve higher calibration accuracy. In addition, the calibration based on the observability index can achieve high calibration accuracy and only requires a limited number of measurement poses.

To calculate observability indices, the singular value decomposition (SVD) of the identification Jacobian matrix $\boldsymbol{J}_\mathrm{B}$ is required:

$$\boldsymbol{J}_B = \boldsymbol{U}\Sigma\boldsymbol{V}^T \tag{30}$$

Then, substituting Equation (30) into Equation (27) yields:

$$d\boldsymbol{q}_B = \boldsymbol{U}\Sigma\boldsymbol{V}^T d\boldsymbol{C} \tag{31}$$

where:

$$\Sigma = \begin{bmatrix} \boldsymbol{S} \\ \boldsymbol{O} \end{bmatrix} \tag{32}$$

where $\boldsymbol{S}$ = diag (σ_1, σ_2, … , σ_L) is a diagonal matrix composed of singular values of $\boldsymbol{J}_\mathrm{B}$. σ_1 and σ_L are the maximum and minimum singular values, respectively. L denotes the number of kinematic parameters. $\boldsymbol{O}$ is a 0 matrix; the size of $\boldsymbol{O}$ is $(6n - 42) \times 42$. According to the geometric significance of SVD, as shown in Figure 3, if the kinematic parameter error vector d$\boldsymbol{C}$ is on the surface of a hypersphere with a unit radius, then the pose error vector d$\boldsymbol{q}_\mathrm{B}$ is on the surface of an L-dimensional hyperellipsoid. The semi-axes length of the

hyperellipsoid is $\sigma_1, \sigma_2, \ldots, \sigma_L$, the singular values of the identification Jacobian matrix. The principles of observability indices can be explained geometrically.

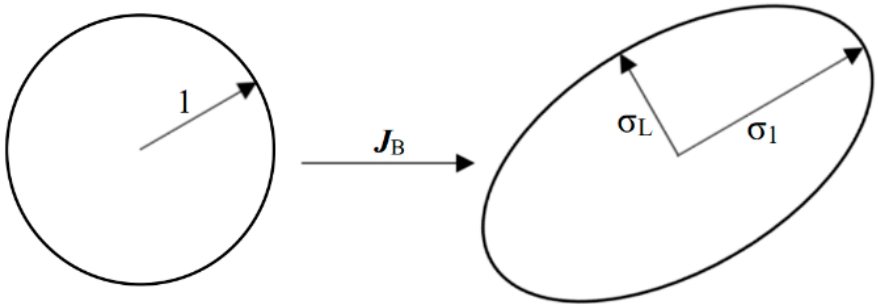

Figure 3. Geometric significance of singular values.

The properties of SVD also reveal the following relationship between the norms of d$\boldsymbol{q}_B$ and d$\boldsymbol{C}$:

$$\sigma_L \leq \frac{|d\boldsymbol{q}_B|}{|d\boldsymbol{C}|} \leq \sigma_1 \tag{33}$$

The measurement noise is determined by the measurement equipment and pose resolving method, so the level of the measurement noise remains unchanged during the calibration process. In addition, the kinematic parameter error vector d$\boldsymbol{C}$ is constant. Therefore, the larger the value of $|\mathrm{d}\boldsymbol{q}_B|$, the smaller the proportion of measurement noise in d$\boldsymbol{q}_B$. The smaller the proportion, the smaller the negative impact of measurement noise, and the higher the accuracy of kinematic calibration.

The first observability index O_1 is calculated as follows:

$$O_1 = \frac{\sqrt[L]{\sigma_1 \sigma_2 \cdots \sigma_L}}{\sqrt{n}} \tag{34}$$

O_1 is the geometric mean of singular values, which is proportional to the volume of the hyperellipsoid in Figure 3. Maximizing O_1 requires the volume of the hyperellipsoid to be as large as possible, which will increase the pose error d$\boldsymbol{q}_B$ in general [18,19]. However, O_1 has some shortcomings: it cannot be guaranteed that the d$\boldsymbol{q}_B$ vector will be inevitably large in a large hyperellipsoid. There is a possibility that the minimum semi-axes of a large hyperellipsoid is very small, and it is theoretically possible to make d$\boldsymbol{q}_B$ as small as the minimum semi-axes [22].

$$O_2 = \frac{\sigma_L}{\sigma_1} \tag{35}$$

O_2 is a measure of the eccentricity of the d$\boldsymbol{q}_B$ hyperellipsoid [20]. The larger the O_2, the closer the hyperellipsoid is to the hypersphere, which will result in the uniformity of singular values. This measure does not consider the volume of the hyperellipsoid, but rather considers its eccentricity.

$$O_3 = \sigma_L \tag{36}$$

Maximizing O_3 requires a large minimum semi-axes of the hyperellipsoid [21]. Maximizing O_3 will increase the minimum semi-axes and volume of the hyperellipsoid, making the selected measurement poses more sensitive to the errors of kinematic parameters.

$$O_4 = \frac{{\sigma_L}^2}{\sigma_1} \tag{37}$$

O_4 is the square of the minimum singular value of the identification Jacobian matrix divided by the maximum singular value, and is the product of O_2 and O_3. Maximizing O_4

will make the minimum semi-axes of the hyperellipsoid larger, and make the maximum semi-axes smaller. In addition, it results in a smaller eccentricity [22].

$$O_5 = \frac{1}{\left(\frac{1}{\sigma_1} + \frac{1}{\sigma_2} + \cdots + \frac{1}{\sigma_L}\right)} \tag{38}$$

O_5 is the reciprocal sum of all singular values, and then takes the reciprocal. It is the harmonic mean divided by the number of parameters L [23].

In general, the larger the value of observability index, the more sensitive the pose error $\mathrm{d}\boldsymbol{q}_\mathrm{B}$ is to the variation of the kinematic parameter error $\mathrm{d}\boldsymbol{C}$, and the smaller the impact of measurement noise. Therefore, a group of poses with larger observability index are more likely to achieve higher calibration accuracy.

However, there is currently no consensus on the performance of the five observability indices. In order to determine which index is most advantageous for the kinematic calibration of the six-hardpoint positioning mechanism, this paper has conducted many numerical simulations of calibration and compared their performance. Finally, we will use the best performance observability index for the calibration method.

3.2. Algorithm for Selecting Measurement Pose

In order to select a group of poses that maximize a certain observability index from many poses, we need a selection algorithm. We considered the DETMAX algorithm [32], which was proposed and used to maximize the determinant of the covariance matrix. The algorithm uses the method of exchanging design points in the initial set and candidate point set multiple times to improve the performance of the initial set, and finally obtains the best solution. The algorithm is widely used in the design of experiments, and the principle of this algorithm is as follows:

① Set the candidate point set to **p** and select the initial solution **s**.
② Select an element from **p** and add it to **s** to maximize the performance of **s**.
③ Remove an element from **s** and return it to **p** to maximize the performance of **s**.
④ Repeat steps ② and ③, and the termination condition is that the added element and the removed element are the same. This algorithm will improve the performance of **s**.

After applying this algorithm to measurement pose selection, it is found that the algorithm has extremely fast convergence speed, and the observability index of the selected poses is indeed higher than the index of the initial poses. However, two problems of this algorithm were found. The first is that it is easy to converge to a local optimal solution, and the second is that the obtained results are greatly affected by initial values. Therefore, this article uses tabu search to improve the DETMAX algorithm, and the improved algorithm adds a tabu list to store a certain number of poses that have been temporarily eliminated during the iteration process. The above improvements effectively avoid the two problems of DETMAX. The process of the improved DETMAX algorithm is as follows:

① Assume that there are 10,000 primary mirror poses to be selected. Let the set of 10,000 primary mirror poses be Ω_0. Extract n poses from Ω_0 as the initial pose set ζ_n, and extract m poses as the initial tabu list η_m. Then the set Ω_0 becomes set Ω, and there are 10,000-n-m poses in Ω.
② Extract a pose from Ω and add it to ζ_n to form $\zeta_{\mathrm{n}+1}$, and calculate the observability index of $\zeta_{\mathrm{n}+1}$. Perform this step for all 10,000-n-m poses in Ω, retain the pose that maximizes the observability index, and the $\zeta_{\mathrm{n}+1}$ corresponding to this pose. There are $n+1$ poses in $\zeta_{\mathrm{n}+1}$. Then the set Ω becomes $\Omega-$ and there are 9999-n-m poses in $\Omega-$.
③ Remove a pose from $\zeta_{\mathrm{n}+1}$, to obtain ζ_n. Calculate the observability index of ζ_n. Perform this step for all $n+1$ poses in $\zeta_{\mathrm{n}+1}$, retain the ζ_n that maximizes the observability index. Record the pose that was removed from $\zeta_{\mathrm{n}+1}$ in the last position of the tabu list η_m. Then, remove the first pose of the η_m, and add the pose to $\Omega-$ to form Ω. Now, there are n poses in ζ_n.

④ Return to step ② and continue to execute until the maximum number of iterations is reached. Finally, the n poses in set ζ_n are the optimal measurement pose that maximize the observability index.

In order to compare the performance of the improved DETMAX algorithm with the traditional DETMAX algorithm, two algorithms were used to select the poses, and the results are shown in Table 1. The results of observability indices of the selected poses indicate that the improved DETMAX algorithm has obtained bigger observability indices, therefore, the improved DETMAX algorithm has better performance.

Table 1. Performance comparison between improved DETMAX algorithm and traditional DETMAX algorithm.

Algorithm		**Improved DETMAX**			**Traditional DETMAX**		
Number of poses		20	30	40	20	30	40
Results	O_1	0.0357	0.0361	0.0362	0.0352	0.0355	0.0355
	O_2	2.459×10^{-4}	2.457×10^{-4}	2.463×10^{-4}	2.432×10^{-4}	2.443×10^{-4}	2.441×10^{-4}
	O_3	1.395×10^{-3}	1.709×10^{-3}	1.973×10^{-3}	1.393×10^{-3}	1.707×10^{-3}	1.970×10^{-3}
	O_4	3.413×10^{-7}	4.165×10^{-7}	4.784×10^{-7}	3.337×10^{-7}	4.104×10^{-7}	4.738×10^{-7}
	O_5	4.361×10^{-4}	5.399×10^{-4}	6.255×10^{-4}	4.314×10^{-4}	5.379×10^{-4}	6.247×10^{-4}

4. Performance Comparison of Observability Indices

In order to improve the accuracy of the proposed calibration method for six-hardpoint positioning mechanisms, this paper attempts to find the most suitable observability index for this mechanism. Therefore, many simulations of calibration have been conducted for this mechanism, and the performance of the five observability indices have been compared.

4.1. The Process of Numerical Simulation of Kinematic Calibration

The error model Equation (27) is accurate only if the kinematic parameter error d$\boldsymbol{C}$ is minimal. Therefore, if the d$\boldsymbol{C}$ is large, it is necessary to gradually modify the theoretical kinematic parameters iteratively to make them gradually approach the actual kinematic parameters, and ultimately complete the calibration. The simulation of kinematic calibration includes three parts: measurement pose selection, generating measurement value of the primary mirror poses, and identification and compensation of kinematic parameter errors. The calibration process is shown in Figure 4 and explained as follows:

① The initial theoretical kinematic parameter $\boldsymbol{C}$ of the six-hardpoint positioning mechanism is known, and the initial kinematic model K is established based on $\boldsymbol{C}$. K includes forward and inverse kinematic models. Then, substitute the initial theoretical pose set $\boldsymbol{q}_B$ obtained using the improved DETMAX algorithm into the inverse kinematic model. Then, obtain n groups of theoretical lengths of hardpoints $\boldsymbol{H}_1$~$\boldsymbol{H}_n$. Let k = 1, $\Delta_0 = 0$.

② Superimpose the preset kinematic parameter error $\boldsymbol{C}_0$ onto $\boldsymbol{C}$ to obtain the actual kinematic parameter $\boldsymbol{C}'$. Establish the kinematic model K$'$ based on $\boldsymbol{C}'$. Substitute $\boldsymbol{H}_1$~$\boldsymbol{H}_n$ into the forward kinematic model based on K$'$, then obtain the actual pose $\boldsymbol{q}_{B1}$ of the primary mirror. Superimpose the measurement noise $\delta\boldsymbol{q}_B$ onto $\boldsymbol{q}_{B1}$ to obtain the measured value $\boldsymbol{q}_B{}'$ of the pose of the primary mirror. Finally, the pose error d$\boldsymbol{q}_B$ of the primary mirror is calculated.

③ Substitute $\boldsymbol{H}_1$~$\boldsymbol{H}_n$, $\boldsymbol{q}_B$, d$\boldsymbol{q}_B$, and $\boldsymbol{C}$ into the Equation (27) and solve it using the least squares method to obtain the identification result of the kinematic parameter error d$\boldsymbol{C}$.

④ $\boldsymbol{C}$ is modified with d$\boldsymbol{C}$ to obtain the modified theoretical kinematic parameter $\boldsymbol{C}''$.

⑤ Using $\boldsymbol{C}''$ to establish a new theoretical kinematic model K″. Substitute $\boldsymbol{H}_1$~$\boldsymbol{H}_n$ into the forward kinematic model based on K″, and a new primary mirror theoretical pose $\boldsymbol{q}_B''$ is obtained. The deviation between $\boldsymbol{q}_B''$ and $\boldsymbol{q}_B{}'$ is d$\boldsymbol{q}_B''$. Calculating the sum of squares of elements in d$\boldsymbol{q}_B''$, record as Δ_k. If $|\Delta_k - \Delta_{k-1}| < \varepsilon$, then the iteration ends, otherwise continue with step ⑥.

⑥ Let $d\boldsymbol{q}_B = d\boldsymbol{q}_B''$, $\boldsymbol{q}_B = \boldsymbol{q}_B''$, $\boldsymbol{C} = \boldsymbol{C}''$, and k = k + 1. Then, return to step ③ and continue to execute, until the condition in step ⑤ is met, then end the iteration.

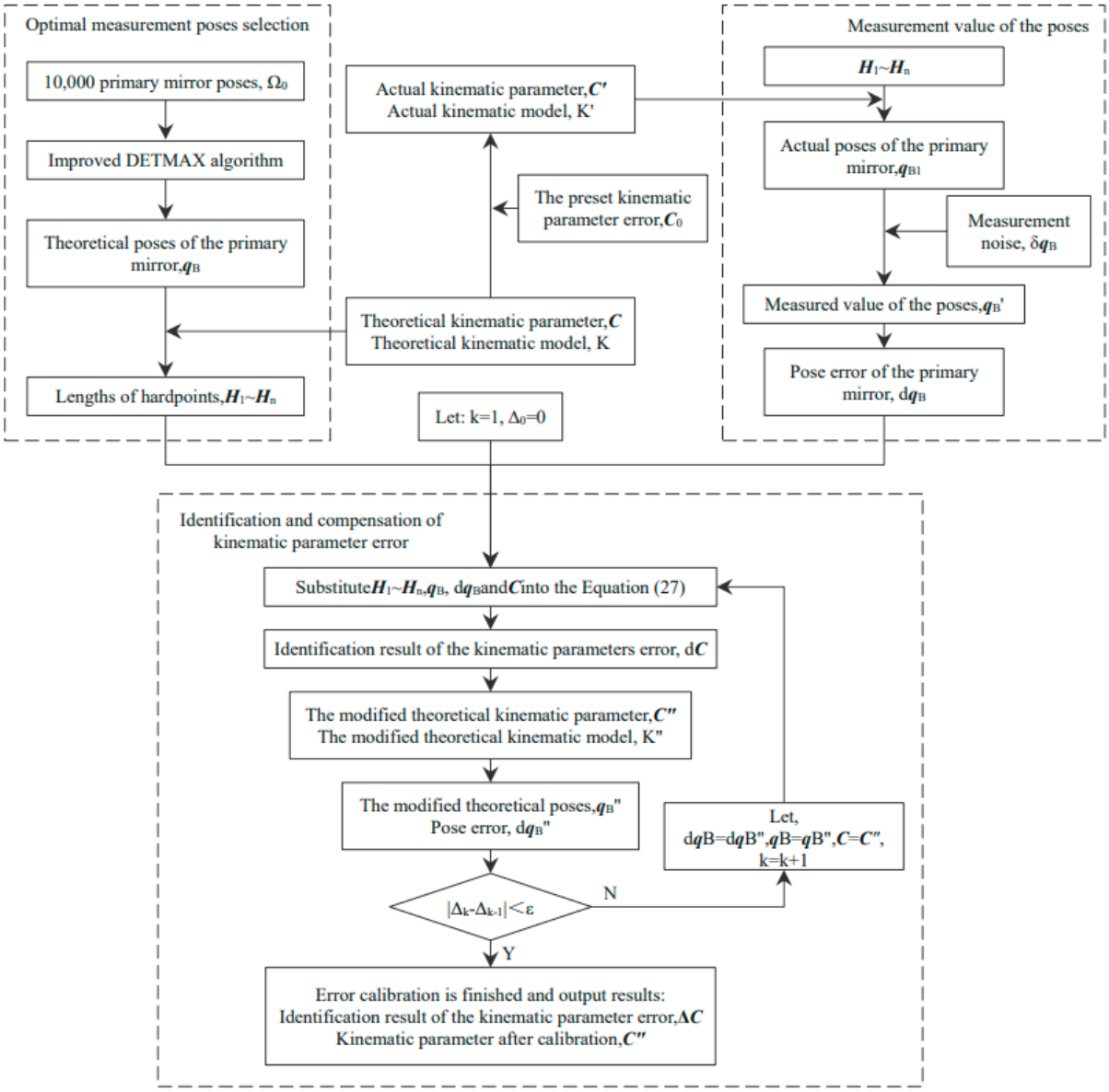

Figure 4. Process diagram of numerical simulation of kinematic calibration for six-hardpoint positioning mechanisms.

After the iteration, calculate the difference between $\boldsymbol{C}''$ and $\boldsymbol{C}$, then the result $\Delta\boldsymbol{C}$ represents the identification result of the kinematic parameter error of the six-hardpoint positioning mechanism. $\boldsymbol{C}''$ is the kinematic parameter after calibration and the kinematic model K″ based on $\boldsymbol{C}''$ is the kinematic model after calibration.

4.2. Evaluation Index of Calibration Accuracy

This paper proposes to evaluate the accuracy of a calibration using the integrated error of the pose of the primary mirror. The integrated error is used to compare the accuracy of multiple calibrations. Preset the 30 target poses of the primary mirror $\boldsymbol{X}i$ (i = 1, 2, . . . , 30), $\boldsymbol{X}i$ evenly distributed in the workspace of the six-hardpoint positioning mechanism. Compare

actual pose $\boldsymbol{Xi'}$ with $\boldsymbol{Xi}$, the deviation can indicate the calibration accuracy. Calculate the pose error of the primary mirror d$\boldsymbol{Xi}$:

$$d\boldsymbol{Xi} = \boldsymbol{Xi'} - \boldsymbol{Xi} \tag{39}$$

where:

$$d\boldsymbol{Xi} = \begin{bmatrix} dx_i & dy_i & dz_i & d\alpha_i & d\beta_i & d\gamma_i \end{bmatrix} \tag{40}$$

d$\boldsymbol{X}_i$ is composed of position error vector [dx_i dy_i dz_i] and attitude error vector [dα_i dβ_i dγ_i]. Calculate the norms dXtn$_i$ and dXsn$_i$ of the two vectors, and then calculate the sum dXzn$_i$ (i = 1, 2, . . . , 30) of the two norms:

$$dXtn_i = \sqrt{dx_i{}^2 + dy_i{}^2 + dz_i{}^2} \tag{41}$$

$$dXsn_i = \sqrt{d\alpha_i{}^2 + d\beta_i{}^2 + d\gamma_i{}^2} \tag{42}$$

$$dXzn_i = dXtn_i + dXsn_i \tag{43}$$

Finally, calculate the root mean square of dXzn$_i$ to obtain the integrated error dXz of the calibration:

$$dXz = \sqrt{\frac{\sum_{i=1}^{20} dXzn_i{}^2}{30}} \tag{44}$$

The accuracy of a calibration can be evaluated with the integrated error dXz, and it is dimensionless.

4.3. Methods for Performance Comparison of Observability Indices

In order to compare the performance of five observability indices in the kinematic calibration of six-hardpoint positioning mechanisms, a numerical simulation method for performance comparison was designed. The method is based on the measurement pose selection algorithm in Section 3.2, the numerical simulation method in Section 4.1, and the accuracy evaluation index in Section 4.2. The performance of the observability index is compared through the accuracy of many simulations of calibration under various conditions. In simulation, the theoretical kinematic parameters of the six-hardpoint positioning mechanism are shown in Table 2.

Table 2. Theoretical kinematic parameters of the six-hardpoint positioning mechanism (unit: mm).

i	x_{Ai}	y_{Ai}	z_{Ai}	x_{Bi}	y_{Bi}	z_{Bi}	h_i
1	421.1	−112.8	0	388.9	−388.9	0	388
2	421.1	112.8	0	388.9	388.9	0	388
3	−112.8	421.1	0	142.4	531.3	0	388
4	−308.3	308.3	0	−531.3	142.4	0	388
5	−308.3	−308.3	0	−531.3	−142.4	0	388
6	−112.8	−421.1	0	142.4	−531.3	0	388

In order to make the conclusions more universal, various measurement conditions were set in the simulation to comprehensively evaluate the performance of observability indices in the calibration of six-hardpoint positioning mechanisms. The measurement conditions refer to the number of measurement poses n and the level of measurement noise. The number of poses should meet the condition of $n \geq 7$. In addition, in order to ensure the efficiency of simulation, n cannot be too large. Finally, the range of n is determined to be 10 to 30. The level of measurement noise mainly depends on the measurement method. Length gauges, laser trackers, linear variable differential transformers (LVDT), measuring

arms, etc., can be used to measure the pose of the primary mirror [29–32], and different pose resolving methods are required. Different equipment and resolving method can lead to different measurement noise. The final determination of the measurement noise range is ±3~±100 μm. In summary, simulations of calibration is performed under the four measurement conditions shown in Table 3. Compare the performance of five observability indices by comparing their calibration accuracy under each condition.

Table 3. Four measurement conditions in the numerical simulation of the kinematic calibration.

No.	Number of Measurement Poses	Measurement Noise (Position, Attitude)
I	10	0.003 mm, 0.0003°
II	15	0.05 mm, 0.005°
III	22	0.01 mm, 0.001°
IV	30	0.1 mm, 0.01°

In order to make the conclusion more universal, 100 sets of kinematic parameter errors were randomly set. The parameter errors present a normal distribution with a standard deviation of 0.5 mm.

The process and method of performance comparison are as follows:

- Generate 100 sets of kinematic parameter errors $\boldsymbol{C}_{0j}$ (j = 1, 2, . . . , 100), with 42 errors per set. Set 10,000 primary mirror poses evenly distributed in the workspace as the poses to be selected.

LOOP 1: For each measurement condition, do:

- The measurement noise matrix is generated based on the measurement condition, and the size of the matrix is $n \times 6$;

LOOP 2: For each observability index, do:

- The improved DETMAX algorithm is used to select n poses that maximize observability index, to obtain the optimal measurement poses.

LOOP 3: For each $\boldsymbol{C}_{0j}$ (j = 1, 2, . . . , 100), do:

- Calculate the actual kinematics parameter $\boldsymbol{C}'$ corresponding to $\boldsymbol{C}_{0j}$.
- Execute the calibration procedure in Section 4.1 to identify kinematic parameter errors, to obtain the corrected kinematic parameter $\boldsymbol{C}''$, and establish the corrected kinematic model K".
- Calculate the integrated error dXz_j (j = 1, 2,..., 100) for this calibration.

END LOOP 3

- Calculate the mean value dXz_{mean} of the integrated error dXz_j (j = 1, 2, . . . , 100).

END LOOP 2

- Produce the histogram superposition probability density function (PDF) curves of the integrated error dXz_j, and compare the performance of observability indices under the current measurement condition.

END LOOP 1

- Use a table to summarize and record the values of mean integrated error dXz_{mean} of each of the five observability indices under four measurement conditions.

In order to comprehensively evaluate the performance of the five observability indices, this paper not only used a table to record the mean integrated errors corresponding to each observability index, but also used histogram superposition PDF curves for performance comparison. The figures and tables represent the comprehensive performance of each observability index in a large number of calibrations. The above method requires 400 simulations of calibration using each observability index, which is equivalent to a total of 2000 calibrations. It can ensure that the conclusion has statistical significance and high reliability.

4.4. Results of Observability Index Performance Comparison

The results of performance comparison of observability indices are shown in Table 4 and Figure 5. Table 4 lists the mean integrated errors of calibration with different observability indices. Figure 5a–d show the histogram superimposed PDF curve of integrated error under each measurement condition. The horizontal coordinate axis in the figure is the value of the integrated error. The left axis is frequency, which corresponds to the histogram, and the right axis is the probability density, which corresponds to the PDF curve.

Table 4. Mean integrated error of calibration with five observability indices.

Measurement Condition	Observability Index	dXz_{mean}
I	O_1	0.01050
	O_2	0.02936
	O_3	0.03388
	O_4	0.04805
	O_5	0.01727
II	O_1	0.15785
	O_2	0.24408
	O_3	0.15933
	O_4	0.22564
	O_5	0.24932
III	O_1	0.02415
	O_2	0.06181
	O_3	0.04541
	O_4	0.05333
	O_5	0.02554
IV	O_1	0.21662
	O_2	0.36087
	O_3	0.27937
	O_4	0.32318
	O_5	0.27659

When analyzing the graphs and tables, taking measurement condition I as an example, Figure 5a shows that after 100 calibrations with five observability indices, respectively, the calibration with O_1 obtains the smallest integrated error overall. Table 4 records that, in measurement conditions I, the mean integrated error of 100 calibrations with O_1 is 0.01050, which is smaller than the mean integrated error corresponding to the other 4 observability indices. Figure 5a also shows that the calibration with O_4 has the largest integrated error. Figure 5b–d show that calibrations with O_1 also have the smallest integrated error in measurement conditions II, III, and IV.

According to the above analysis, the simulations of calibrations of the six-hardpoint positioning mechanism with O_1 obtains the minimum integrated error and the highest accuracy. Therefore, we believe that O_1 has better performance than the other four observability indices, and O_1 is the most suitable observability index for calibration of six-hardpoint positioning mechanisms. In the proposed calibration method, the index O_1 is used to select the optimal measurement poses.

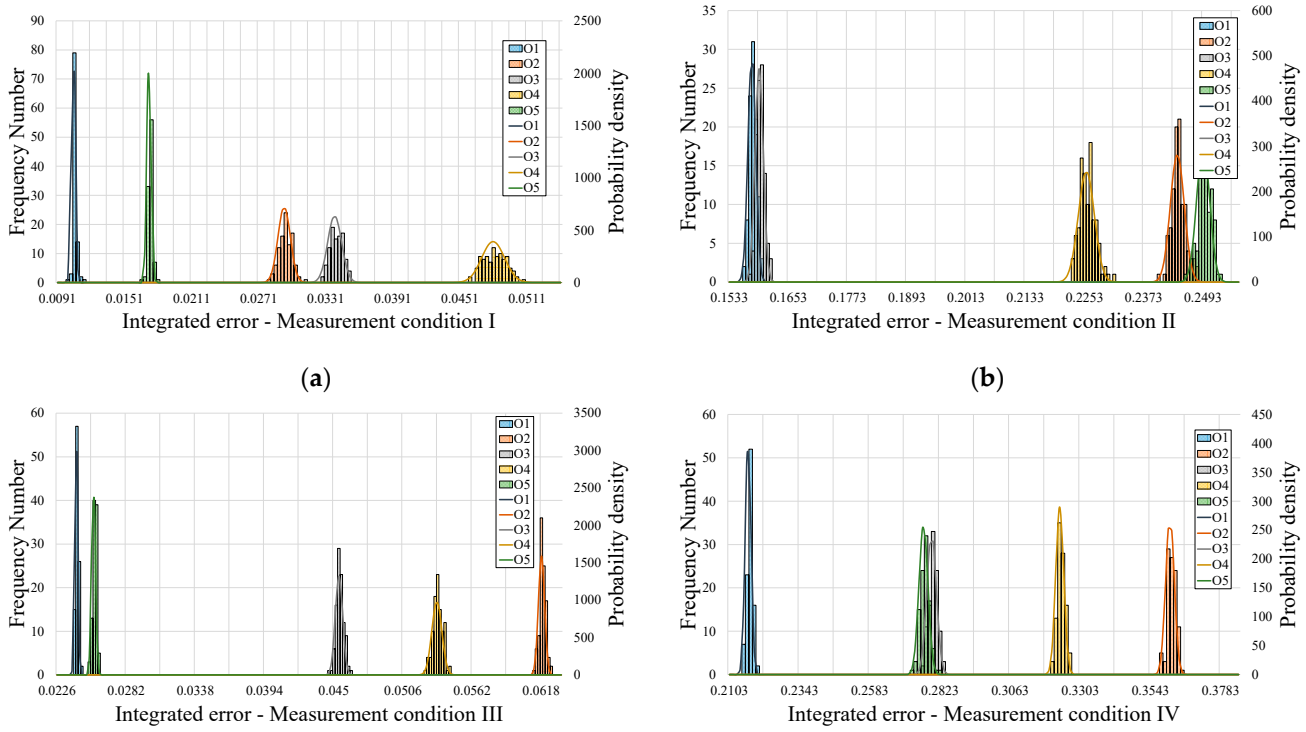

(**a**) (**b**)

(**c**) (**d**)

Figure 5. Histogram superimposed PDF curve of integrated error of simulations of calibration. (**a**) Measurement condition I; (**b**) Measurement condition II; (**c**) Measurement condition III; (**d**) Measurement condition IV.

5. Evaluation and Discussion of the Kinematic Calibration Method Using Optimal Measurement Pose

In order to evaluate the proposed kinematics calibration method of six-hardpoint positioning mechanisms using optimal measurement pose, the simulations of calibrations using the proposed method and traditional calibration method were performed under the same conditions. The same conditions refer to the same kinematic parameter errors and the same measurement noise. To eliminate chance, a new set of initial configuration parameters were used, as shown in Table 5. The set kinematic parameter error is shown in Table 6. The randomly generated parameter error assumes a normal distribution with a standard deviation of 0.5 mm. The measurement noise of the pose of the primary mirror is also normally distributed, with a standard deviation of 0.001 mm. The theoretical kinematic parameters and kinematic parameter errors are superimposed to simulate the actual kinematic parameters, and the measurement noise is superimposed on the actual pose of the primary mirror to obtain the measurement value of the pose. The number n of the measurement poses is 20.

Table 5. New theoretical kinematic parameters (unit: mm).

i	x_{Ai}	y_{Ai}	z_{Ai}	x_{Bi}	y_{Bi}	z_{Bi}	h_i
1	1299.170	−348.112	0	1164.388	−977.037	0	800
2	1299.170	348.112	0	1164.388	977.037	0	800
3	−348.112	1299.170	0	263.945	1496.908	0	800
4	−951.059	951.059	0	−1428.333	519.871	0	800
5	−951.059	−951.059	0	−1428.333	−519.871	0	800
6	−348.112	−1299.170	0	263.945	−1496.908	0	800

Table 6. Preset values of kinematic parameter errors (unit: mm).

i	$\mathrm{d}x_{Ai}$	$\mathrm{d}y_{Ai}$	$\mathrm{d}z_{Ai}$	$\mathrm{d}x_{Bi}$	$\mathrm{d}y_{Bi}$	$\mathrm{d}z_{Bi}$	$\mathrm{d}h_i$
1	−0.5	−0.2	−1	−0.4	0.2	0.6	0.6
2	0.1	−0.3	−0.7	0.4	0.2	−0.3	−0.1
3	0	−0.4	−0.3	−0.1	−0.3	0.7	0.1
4	0.3	1.1	−0.2	−0.1	−0.7	0.2	−0.2
5	−0.4	0.3	−0.7	−1.3	0.8	0.7	0.3
6	−0.9	−0.2	1.1	0.4	−0.4	−0.3	−0.2

The proposed calibration method requires selecting the optimal measurement poses based on the observability index O_1. Therefore, the improved DETMAX algorithm was used to select 20 poses from 2000 poses to be selected, with the criteria of maximizing O_1. The 2000 poses are evenly distributed in the workspace. In the algorithm, the size of the tabu list is set to 100, resulting in 20 optimal measurement poses. The observability index of the optimal measurement poses was O_1 = 0.03571. After 219 iterations, the result was obtained. The variation of O_1 during the selection process is shown in Figure 6. When using the traditional DETMAX algorithm, the result is obtained by only 21 iterations, and the obtained value of O_1 is smaller than the value obtained by the improved DETMAX algorithm. The improved DETMAX algorithm improves the problem of convergence to the local optimal solution.

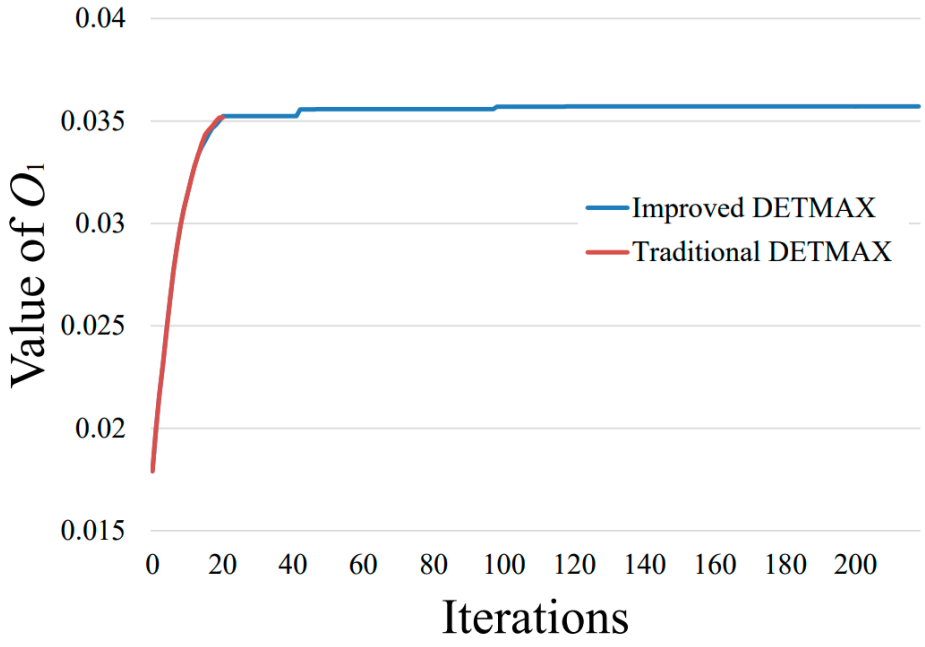

Figure 6. The process of measurement poses selection using improved DETMAX algorithm and traditional DETMAX algorithm.

In order to ensure the effectiveness of the improved DETMAX algorithm, 1000 sets of poses were randomly selected from 2000 poses, and each set has 20 poses. The observability index O_1 corresponding to each set was calculated and the results were plotted as a histogram, as shown in Figure 7. The maximum value of O_1 corresponding to these sets is 0.02199, and the average value is 0.01713. The results show that the value of O_1 has been maximized, and the improved DETMAX algorithm performs well.

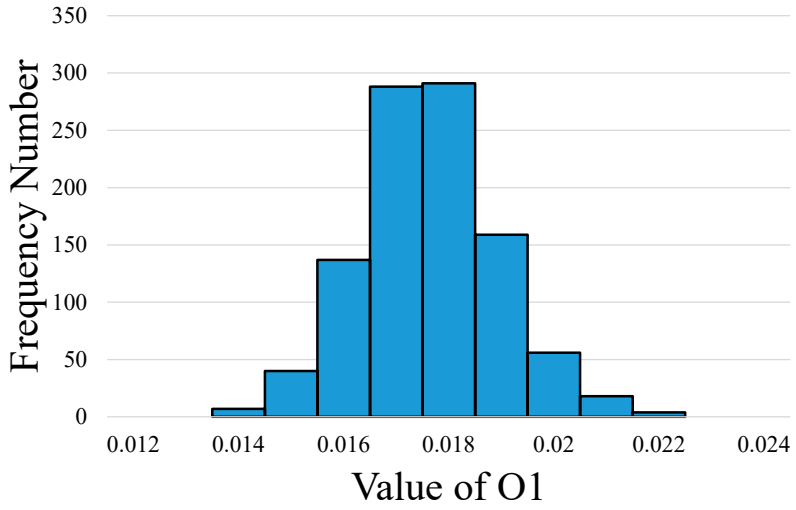

Figure 7. Results of the observability index O_1 corresponding to 1000 sets of random poses.

The optimal measurement poses are used for calibration. During the calibration process, the variation of kinematic parameter errors during the iteration process are shown in Figure 8. Due to space constraints, only seven kinematic parameter errors related to the first hardpoint are given in the figure. After three iterations, the error value tends to be stable and the convergence speed of the calibration is fast. The identification results of all kinematic parameter errors are shown in Table 7.

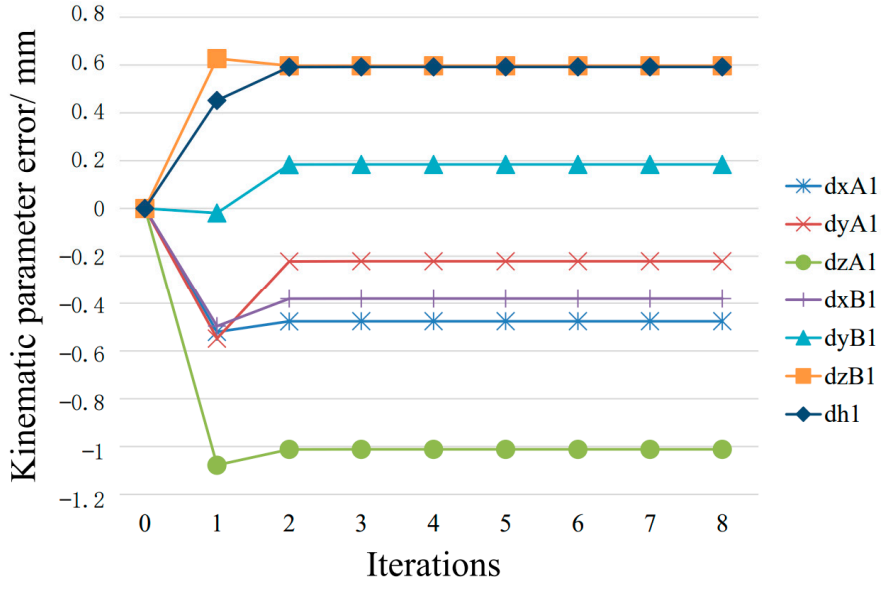

Figure 8. The variation of kinematic parameter errors during the calibration.

Table 7. Identification results of kinematic parameter errors.

i	$\mathrm{d}x_{Ai}$	$\mathrm{d}y_{Ai}$	$\mathrm{d}z_{Ai}$	$\mathrm{d}x_{Bi}$	$\mathrm{d}y_{Bi}$	$\mathrm{d}z_{Bi}$	$\mathrm{d}h_i$
1	−0.476	0.134	−0.032	0.275	−0.432	−0.882	−0.476
2	−0.221	−0.275	−0.380	1.121	0.277	−0.232	−0.221
3	−1.012	−0.708	−0.307	−0.200	−0.710	1.104	−1.012
4	−0.381	0.426	−0.162	−0.128	−1.343	0.410	−0.381
5	0.184	0.246	−0.287	−0.686	0.791	−0.430	0.184
6	0.597	−0.324	0.708	0.195	0.678	−0.288	0.597

After obtaining the identification results of the kinematic parameter errors, the theoretical kinematic parameters are modified, and a new kinematic model is established based on the modified parameters. Then, set 150 primary mirror pose targets, and evaluate the result of the calibration. The results obtained by using the proposed calibration method and traditional calibration method were compared. The errors of the 150 poses of the primary mirror are shown in Figure 9. Figure 9a shows the position error, and Figure 9b shows the attitude error. The results in Figure 9 show that the proposed calibration method using the optimal measurement poses achieves significantly higher accuracy than the traditional calibration method, both in position accuracy and attitude accuracy. The above results verify the effectiveness of the proposed calibration method.

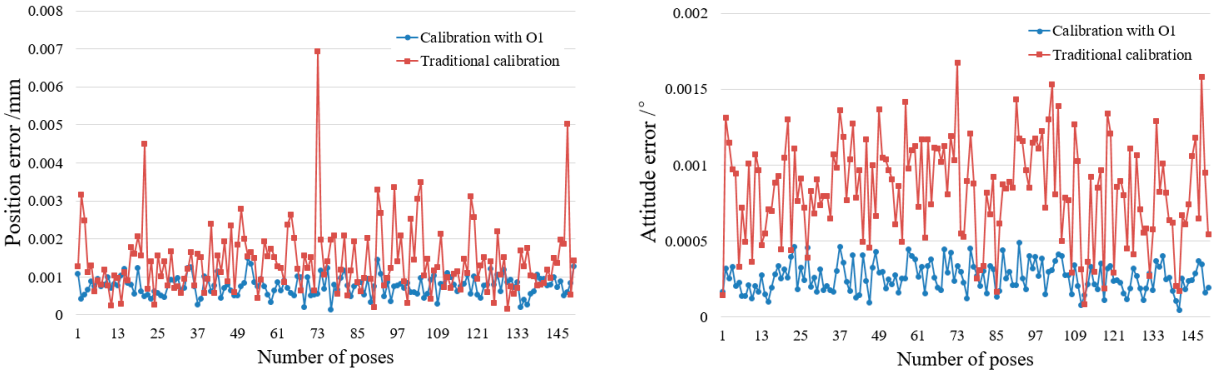

(**a**) (**b**)

Figure 9. Position and attitude errors of 150 primary mirror poses. (**a**) Position errors; (**b**) Attitude errors.

The errors of the proposed calibration method and the traditional calibration method are listed in Table 8. Compared with the traditional method, the mean position error obtained by the proposed method decreases by 78.4%, and the mean attitude error decreases by 70.6%.

Table 8. Position error and attitude error after calibration using two methods.

	Position Error/mm		**Attitude Error/°**	
	Maximum	**Mean**	**Maximum**	**Mean**
Calibration with O_1	0.001498	0.000771	0.000492	0.000262
Traditional calibration	0.006933	0.001424	0.001675	0.000839

The number n of measurement poses in the above calibrations is 20. The number of measurement poses in calibration has been increased, and the results are shown in Figure 10. When using traditional methods, the integrated error decreases significantly as the number of measurement poses increases. When using the proposed calibration method with O_1, there is no significant change in the integrated error by increasing the number of measurement poses. In addition, the proposed calibration using optimal measurement pose based on O_1 requires only 20 measurement poses, which achieves a calibration accuracy approximately equal to the accuracy of traditional calibration methods using 50 measurement poses. The above results show that the proposed calibration method is effective, not only with high accuracy, but also with less measurement poses to achieve high accuracy.

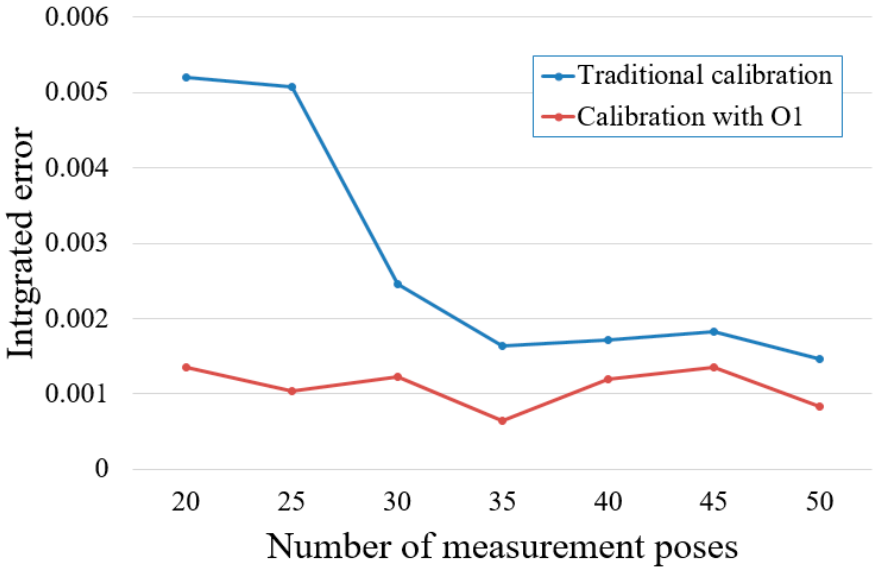

Figure 10. Relationship between integrated error and number of measured poses.

6. Conclusions

This paper proposes a kinematic calibration method using optimal measurement poses based on the observability index O_1, which can be used for six-hardpoint positioning mechanisms to effectively identify and compensate the kinematic parameter errors of the mechanisms, thereby improving the accuracy of the primary mirror pose. The proposed method selects specific measurement poses based on the index O_1 to reduce the negative impact of measurement noise, achieving higher calibration accuracy than the traditional method. Firstly, the error model of the six-hardpoint positioning mechanism is derived. Then, introduce the observability indices and the algorithm for selecting measurement poses based on observability indices. We improved the DETMAX algorithm and used it for measurement poses selection. The performance of the five observability indices was compared through simulations of calibration, and the best performance observability index O_1 was obtained; 2000 simulation calibrations were conducted under different conditions, ensuring that the results were statistically significant. Finally, an overall evaluation of the proposed calibration method was conducted, and the results obtained by the proposed calibration method and the traditional calibration method were compared. The results show that the proposed calibration method can accurately identify kinematic parameter errors, and has higher accuracy compared with the traditional method. The mean position error decreased by 78.4%, and the mean attitude error decreased by 70.6%. The proposed method can be used to improve the kinematic accuracy of six-hardpoint positioning mechanisms. There are two main aspects of future work planning. This paper mainly studies the kinematics parameter error and measurement noise. We will study other factors that affect the accuracy of the six-hardpoint positioning mechanism in future work, such as thermal deformation and gravity deformation. In addition, we will study the observability index and kinematics calibration on more types of robots.

Author Contributions: Conceptualization, Z.Y.; methodology, Z.Y. and X.W.; software, Z.Y.; validation, Z.Y., X.W. and F.W.; data curation, Z.Y.; writing—original draft preparation, Z.Y.; writing—review and editing, Z.Y., X.W. and F.W.; supervision, F.W.; funding acquisition, X.W. All authors have read and agreed to the published version of the manuscript.

Funding: This research was funded by the National Natural Science Foundation of China (No. 12133009).

Institutional Review Board Statement: Not applicable.

Informed Consent Statement: Not applicable.

Data Availability Statement: All data included in this study are available upon request by contacting the corresponding author.

Conflicts of Interest: The authors declare no conflict of interest.

References

1. Crass, J.; Bechter, A.; Sands, B.; King, D.; Ketterer, R.; Engstrom, M.; Hamper, R.; Kopon, D.; Smous, J.; Crepp, J.R.; et al. Final design and on-sky testing of the iLocater SX acquisition camera: Broad-band single-mode fibre coupling. *Mon. Not. R. Astron. Soc.* **2021**, *501*, 2250–2267. [CrossRef]
2. Meeks, R.L.; Ashby, D.; Biddick, C.; Devries, J.; Gusick, M.; Kern, J. Super hardpoints for the Large Binocular Telescope. *Proc. SPIE* **2010**, *7733*, 1888–1900. [CrossRef]
3. Yin, J.E.; Eisenstein, D.J.; Finkbeiner, D.P.; Stubbs, C.W.; Wang, Y. Active Optical Control with Machine Learning: A Proof of Concept for the Vera C. Rubin Observatory. *Astron. J.* **2021**, *161*, 216. [CrossRef]
4. Neill, D.; Angeli, G.; Claver, C.; Hileman, E.; DeVries, J.; Sebag, J.; Xin, B. Overview of the LSST active optics system. *Proc. SPIE* **2014**, *9150*, 143–158. [CrossRef]
5. Dam, M.A.; McLeod, B.A.; Bouchez, A.H. Dispersed fringe sensor for the Giant Magellan Telescope. *Appl. Optics* **2016**, *55*, 539–547. [CrossRef]
6. Aguayo, F.; Ashby, D.; Bugueno, E.; Fischer, B.; Ford, J.; Gray, P.; Gusick, M.; Hebert, A.; Kechichian, Z.; Ranka, T.; et al. GMT M1 subsystem: Status, design and testing. *Proc. SPIE* **2018**, *10700*, 1001–1012. [CrossRef]
7. Noethe, L.; Guisard, S. Final alignment of the VLT. *Proc. SPIE* **2000**, *4003*, 382–390. [CrossRef]
8. Gu, Z.; Yan, C.; Wang, Y. Alignment of a three-mirror anastigmatic telescope using nodal aberration theory. *Opt. Express* **2015**, *23*, 25182–25201. [CrossRef]
9. Gao, G.; Kuang, L.; Liu, F.; Xing, Y.; Shi, Q. Modeling and Parameter Identification of a 3D Measurement System Based on Redundant Laser Range Sensors for Industrial Robots. *Sensors* **2023**, *23*, 1913. [CrossRef]
10. Wang, Z.; Cao, B.; Xie, Z.; Ma, B.; Sun, K.; Liu, Y. Kinematic Calibration of a Space Manipulator Based on Visual Measurement System with Extended Kalman Filter. *Machines* **2023**, *11*, 409. [CrossRef]
11. Li, F.; Zeng, Q.; Ehmann, K.F.; Cao, J.; Li, T. A calibration method for overconstrained spatial translational parallel manipulators. *Robot. Cim Int. Manuf.* **2019**, *57*, 241–254. [CrossRef]
12. Jiang, Y.; Yu, L.; Jia, H.; Zhao, H.; Xia, H. Absolute Positioning Accuracy Improvement in an Industrial Robot. *Sensors* **2020**, *20*, 4354. [CrossRef] [PubMed]
13. Jia, Y.; Zhang, X.; Wang, Z.; Wang, W. Intelligent Calibration of a Heavy-Duty Mechanical Arm in Coal Mine. *Electronics* **2020**, *9*, 1186. [CrossRef]
14. Yang, L.; Tian, X.; Li, Z.; Chai, F.; Dong, D. Numerical simulation of calibration algorithm based on inverse kinematics of the parallel mechanism. *Optik* **2019**, *182*, 555–564. [CrossRef]
15. Cao, H.Q.; Nguyen, H.X.; Tran, T.N.C.; Tran, H.N.; Jeon, J.W. A Robot Calibration Method Using a Neural Network Based on a Butterfly and Flower Pollination Algorithm. *Ieee. T. Ind. Electron.* **2022**, *69*, 3865–3875. [CrossRef]
16. Moser, B.L.; Gordon, J.A.; Petruska, A.J. Unified Parameterization and Calibration of Serial, Parallel, and Hybrid Manipulators. *Robotics* **2021**, *10*, 124. [CrossRef]
17. Wang, Y.; Li, M.; Wang, J.; Zhao, Q.; Wu, J.; Wang, J. Kinematic Calibration Method for Large-Sized 7-DoF Hybrid Spray-Painting Robots. *Machines* **2023**, *11*, 20. [CrossRef]
18. Menq, C.H.; Borm, J.H.; Lai, J.Z. Identification and Observability Measure of a Basis Set of Error Parameters in Robot Calibration. *J. Mech. Design* **1989**, *111*, 513–518. [CrossRef]
19. Borm, J.H.; Meng, C.H. Determination of Optimal Measurement Configurations for Robot Calibration Based on Observability Measure. *Int. J. Robot. Res.* **1991**, *10*, 51–63. [CrossRef]
20. Driels, M.R.; Pathre, U.S. Significance of observation strategy on the design of robot calibration experiments. *J. Robot. Syst.* **1990**, *7*, 197–223. [CrossRef]
21. Nahvi, A.; Hollerbach, J.M.; Hayward, V. Calibration of a parallel robot using multiple kinematic closed loops. In Proceedings of the 1994 IEEE International Conference on Robotics and Automation, San Diego, CA, USA, 8–13 May 1994; Volume 1, pp. 407–412. [CrossRef]
22. Nahvi, A.; Hollerbach, J.M. The noise amplification index for optimal pose selection in robot calibration. In Proceedings of the IEEE International Conference on Robotics and Automation, Minneapolis, MN, USA, 22–28 April 1996; Volume 1, pp. 647–654. [CrossRef]
23. Sun, Y.; Hollerbach, J.M. Observability index selection for robot calibration. In Proceedings of the 2008 IEEE International Conference on Robotics and Automation, Pasadena, CA, USA, 19–23 May 2008. [CrossRef]
24. Le, P.-N.; Kang, H.-J. A New Manipulator Calibration Method for the Identification of Kinematic and Compliance Errors Using Optimal Pose Selection. *Appl. Sci.* **2022**, *12*, 5422. [CrossRef]
25. Saputra, V.B.; Ong, S.K.; Nee, A.Y.C. Optimum calibration of a parallel kinematic manipulator using digital indicators. *Adv. Manuf.* **2014**, *2*, 222–230. [CrossRef]

26. Horne, A.; Notash, L. Comparison of Pose Selection Criteria for Kinematic Calibration through Simulation. *Comput. Kinemat.* **2009**, *1*, 291–298. [CrossRef]
27. Zhou, J.; Kang, H.J.; Ro, Y.S. Comparison of the Observability Indices for Robot Calibration considering Joint Stiffness Parameters. In Proceedings of the Advanced Intelligent Computing Theories and Applications. ICIC 2010. Communications in Computer and Information Science, Changsha, China, 18–21 August 2010; Volume 93, pp. 372–380. [CrossRef]
28. Li, B.; Zhao, H.Y.; Xi, J.P.; Ren, D.X. On-machine self-calibration method for compensation during precision fabrication of 900-mm-diameter zerodur aspheric mirror. *Int. J. Adv. Manuf. Tech.* **2015**, *76*, 1855–1863. [CrossRef]
29. Chen, T.; Lin, J.; Wu, D.; Wu, H. Research of Calibration Method for Industrial Robot Based on Error Model of Position. *Appl. Sci.* **2021**, *11*, 1287. [CrossRef]
30. Lan, B.; Wu, X.; Li, J.; Ming, M.; Liu, X.; Yang, H. Influence of axial-force errors on the deformation of the 4 m lightweight mirror and its correction. *Appl. Optics* **2017**, *56*, 611–619. [CrossRef]
31. Joubair, A.; Slamani, M.; Bonev, I.A. Kinematic calibration of a 3-DOF planar parallel robot. *Ind. Robot.* **2012**, *39*, 392–400. [CrossRef]
32. Mitchell, T.J. An algorithm for the construction of "D-optimal" experimental designs. *Technometrics* **2000**, *42*, 48–54. [CrossRef]